

Article

Plant Extract Induced Biogenic Preparation of Silver Nanoparticles and Their Potential as Catalyst for Degradation of Toxic Dyes

Khalida Naseem ^{1,*}, Muhammad Zia Ur Rehman ², Awais Ahmad ^{3,*} , Deepak Dubal ^{4,*} and Tahani Saad AlGarni ⁵

¹ Department of Chemistry, Faculty of Sciences, University of Central Punjab, Lahore 54000, Pakistan

² Department of Chemical Engineering, University of Engineering and Technology, Lahore 54890, Pakistan; timsheet123@gmail.com

³ Department of Chemistry, The University of Lahore, Lahore 54590, Pakistan

⁴ School of Chemistry, Physics and Mechanical Engineering, Queensland University of Technology, O Block, Level 4, Room O-406, Gardens Point Campus, Brisbane, QLD 4001, Australia

⁵ Chemistry Department, College of Science, King Saud University, Riyadh 11451, Saudi Arabia; Tahanis@ksu.edu.sa

* Correspondence: khalida.naseem@ucp.edu.pk (K.N.); awaisahmed@gcuf.edu.pk (A.A.); deepak.dubal@qut.edu.au (D.D.)

Received: 30 October 2020; Accepted: 14 December 2020; Published: 16 December 2020



Abstract: This study focusses on the synthesis of silver nanoparticles (Ag-nPs) by citrus fruit (*Citrus paradisi*) peel extract as reductant while using AgNO₃ salt as source of silver ions. Successful preparation of biogenic CAg-nPs catalyst was confirmed by turning the colorless reaction mixture to light brown. The appearance of surface Plasmon resonance (SPR) band in UV-Vis spectra further assured the successful fabrication of nPs. Different techniques such as FTIR, TGA and DLS were adopted to characterize the CAg-nPs. CAg-nPs particles were found to excellent catalysts for reduction of Congo red (CR), methylene blue (MB), malachite green (MG), Rhodamine B (RhB) and 4-nitrophenol (4-NP). Reduction of CR was also performed by varying the contents of NaBH₄, CR and catalyst to optimize the catalyst activity. The pseudo first order kinetic model was used to explore the value of rate constants for reduction reactions. Results also interpret that the catalytic reduction of dyes followed the *Langmuir–Hinshelwood* (LH) mechanism. According to the LH mechanism, the CAg-nPs role in catalysis was explained by way of electrons transfer from donor (NaBH₄) to acceptor (dyes). Due to reusability and green synthesis of the CAg-nPs catalyst, it can be a promising candidate for the treatment of water sources contaminated with toxic dyes.

Keywords: nanoparticles; dyes; catalysis; reduction

1. Introduction

Recently, different environmental pollutants such as toxic dyes have been identified as threats because these dyes are harmful for humans and aquatic life [1,2]. Discharge of these dyes containing effluents in the environment causes the natural ecosystem to become unbalanced [3]. Therefore, the effective removal of toxic dyes from wastewater or their conversation in usable sources before its discharge in the water system is a primary global issue [4]. Different methods like biodegradation, electrochemical, physicochemical and photochemical treatment including the advanced oxidation process via photo-catalysis or chemical reduction, adsorption and ultra-filtration have been adopted to address this problem [5,6]. Most of these methods are not useful for the treatment of dyes' polluted wastewater. Methods such as the physicochemical method are inefficient for degradation of dyes due

to their high stability. The biodegradation method, however, is cost effective, yet it is a very slow method, and dyes are also harmful for microorganisms. Adsorption transfers the toxic dyes from one medium to another rather than eliminating them. However, catalytic degradation of dyes has emerged as the best method for their treatment [1]. Harmful substances can be distrusted into less toxic or non-toxic substances via photo-catalysis [7,8] or chemical catalysis [9]. Various metal nanoparticles like Au, Pt, Pd, Fe and Ag-nPs are reported as catalysts for degradation of various toxic dyes [10–13]. One of the most commonly used metal nPs for direct reduction reactions of pollutants is iron nPs. These nPs are less toxic and cost effective. However, Ag-nPs are more stable and highly active catalysts for reduction reactions.

Among these nPs, silver nanoparticles (Ag-nPs) have been considered as interesting candidates over the last decade due to exceptional properties such as high catalytic activity with controlled surface area and low cost [14–18].

Several synthetic methods such as chemical, photochemical and electrochemical methods have been adopted to prepare Ag-nPs by treatment of silver salt [17,19]. However, these methods involve the use of toxic chemicals along with drastic reaction conditions and induce severe environmental pollutions. Due to negative impacts of these reported methods, a new method for preparation of Ag-nPs by plant extracts has been introduced [20]. Plant extract mediated synthesis of nPs tunes their size, shape and size distribution. The biological method for preparation of nPs exhibits several merits over other reported physiochemical methods such as use of non-toxic solvent (water), no utilization of toxic or harmful chemicals, mild reaction conditions and cost effectiveness. Mostly, plant extracts pose different organic compounds with different functional groups such as amino acid and carboxylic acid that act as stabilizing and reducing agents. Plant extracts also act as reducing and stabilizing agents due to the presence of polyphenols [21]. Size and shape of nPs can also be tuned by changing the contents of plant extract utilized during their preparation. Thus, alternatively, catalytic properties of nPs can also be tuned according to the requirement as catalysis is the surface phenomenon [22]. Due to these reasons, many researchers turned toward the utilization of biological units such as plant extract for preparation and stabilization of metal nPs [21,23]. Gardea-Torresdey et al. successfully fabricated Ag-nPs by growing live alfalfa plants in AuCl_4 rich media and concluded that bio items can be used efficiently for preparation of inorganic nanoparticles [24]. Kasthuri et al. prepared Au-nPs by using the chloroauric acid as source of gold ions in the presence of phyllanthin extract at room temperature [22].

Citrus is one of the major fruit crops that is widely consumed as fresh fruit or juice by removing the peel. Peel of fruits is discarded as waste material. Citrus fruit peel has polyphenolic compounds, flavonoids, ascorbic acid etc. These phytochemical components have bioactive properties like antiproliferation, antibacterial, antifungal, antioxidant and antiviral activities [25]. Due to these functional groups, citrus peel extract also acts as a capping agent. Thus, *Citrus paradisi* peel extract induced nPs remain stable for a prolonged amount of time due to the formation of interaction between these functional groups and nPs [21]. Values of apparent rate constant and reaction completion time for reduction of dyes and aromatic compounds in the presence of different metal nanoparticles stabilized by a variety of plant extract for comparative purpose are given in Table 1. Activity of reported catalysts was high for reduction of different dyes as compared to previously used biogenic metal nanoparticles stabilized by plant extracts.

Many research papers used the *Citrus paradisi* peel extract for preparation of different metal nPs like Fe_3O_4 [26,27], ZnO [28] and Ag-nPs [21,25,28–30]. It acts as a reducing as well as a capping agent during preparation of Ag-nPs. Fabricated CAg-nPs find applications in synthesis of durable cotton and silk fabric due to their antibacterial and antimicrobial activity and essential oil effect due to the use of citrus plant extracts [31]. These nanoparticles also find use as potential bio-pesticides to control different types of pathogens in aqueous medium [25,32].

Table 1. Comparative analysis kinetic parameters for catalytic reduction of different dyes using different plant extract induced metal nanoparticles.

Dye	Catalyst	Plant Extract	k_{app} (min^{-1})	Reaction Completion Time (min)	References
CR	Au-nPs	Salmalia malabarica gum	0.236	10	[10]
	Ag-nPs	Gum tragacanth	0.148	15	[33]
	Ag-nPs	Thunbergia grandiflora	0.099	18	[34]
	Ag-nPs	Citrus paradise	0.591	5	This work
MB	Au-nPs	Salmalia malabarica gum	0.241	9	[10]
	Ag-nPs	Gum tragacanth	0.182	12	[33]
	Ag-nPs	<i>Gmelina arborea</i>	-	10	[35]
	Ag-nPs	Citrus paradise	0.613	4	This work
4-NP	Ag-nPs	Coleus forskohlii root extract	0.101	24	[36]
	Au-nPs	Prunus domestica (plum) fruit extract	0.114	9	[37]
	Ag-nPs	Dolichos lablab	-	40	[38]
	Ag-nPs	Citrus paradise	0.247	9	This work

However, no one used these metal nanoparticles as catalysts for degradation of toxic dyes. Thus, we reported here for the first time the preparation of citrus peel induced biogenic CAg-nPs particles and their use as catalysts for degradation of different toxic dyes like CR, MB, MG, RhB and 4-NP. Recyclability and reusability of catalysts were also performed for reduction of CR. Prepared biogenic CAg-nPs particles were analyzed by UV-Vis, FTIR, DLS and TGA.

2. Materials and Methods

2.1. Materials

Congo red (CR) (98%), methylene blue (MB) (98%), malachite green (MG) (98%), Rhodamine B (RhB) (98%), 4-nitrophenol (4-NP) (98%), sodium borohydride (NaBH_4) (98%) and silver nitrate (AgNO_3) (98%) were purchased from Scharlau (Barcelona, Spain) and used as such without further treatment. Deionized water was used throughout the experimentation. Filtration of plant extract was done by Whatmann No. 1 filter paper (Merck Darmstadt, Germany).

2.2. Synthesis of CAg-nPs

Citrus paradisi peels were washed and completely dried in shade. The dried peels were grinded into fine powder using mortar. Afterward, 0.5 g of fine peel powder was stirred with 80 mL deionized water for 3 h in a flask at 60 °C on hotplate and filtered for further use. After that, a 30 mL peel extract was treated with 30 mL of 1.0 mM AgNO_3 solution at 70 °C for 50 min on a hotplate in a round bottom flask under constant stirring and nitrogen supply. Reaction mixture turned light brown on treatment with plant extract. Afterward, a light brown emulsion type mixture was filtered and saved in a sample bottle covered with aluminum foil for analysis. It was also used as a catalyst for catalytic reduction of toxic dyes. Prepared CAg-nPs were also dried in powdered form for pursuing other analyses. Diagrammatic representation of preparation of biogenic CAg-nPs and their use as catalysts for reduction of CR are shown in Figure 1.

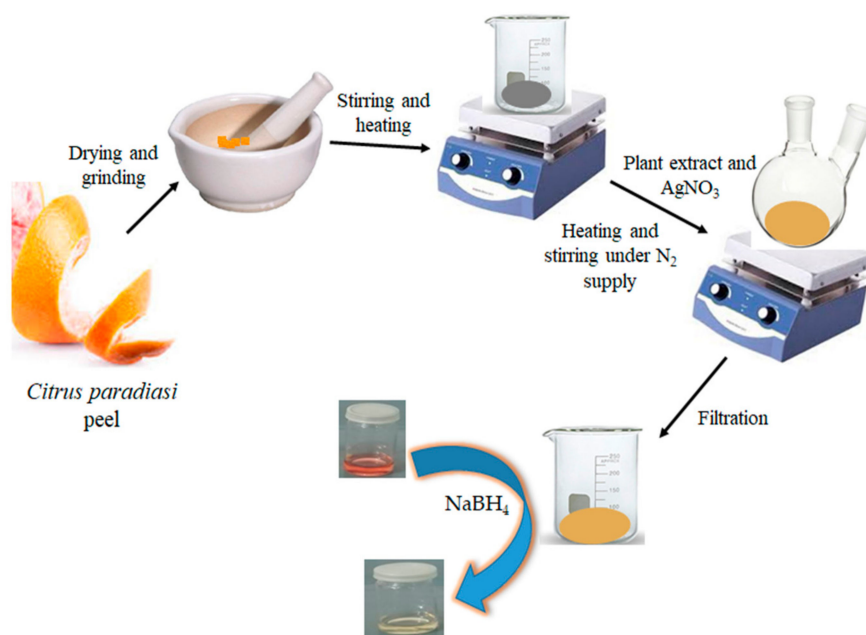


Figure 1. Scheme for preparation of Ag-nPs by the *Citrus paradisi* peel extract and its use as catalyst for reduction of CR.

2.3. Characterization of CAg-nPs

Functional groups of plant extract and biosynthesized CAg-nPs particles were evaluated by scanning FTIR spectra. For this aim, FTIR spectra of powdered samples were scanned on RXI FTIR spectrometer (Perkin ELMER, Waltham, MA, USA). UV-Vis analysis of plant extract, aqueous solution of AgNO₃ and biogenic CAg-nPs particles was also performed on a UV VIS Spectrophotometer (Stalwart, Germany) in the wavelength range from 250 to 750 nm at 25 °C. DLS analysis was done to check the particle size distribution of CAg-nPs particles. For this purpose, analysis was performed on B1-200SM (Brookhaven Instrument Corp, Holtsville, NY, USA at 90° (angle of scattering)) while the He-Ne laser was used as a light source with a wavelength of 637 nm. TGA analysis of plant extract and biogenic CAg-nPs particles was also done on Thermal analyzer (Model: SDT, Q-600, TA Shanghai, China) in the presence of N₂.

2.4. Catalytic Reduction of Toxic Dyes

In addition, 0.060 mM CR and 7.88 mM NaBH₄ were taken in a cuvette along with 1.8 mg/mL of CAg-nPs catalyst and spectra were recorded in the range of 380 to 680 nm with a one minute interval on a UV-Vis spectrophotometer (Stalwart, Dehli India) to check the reaction progress. CR reduction was also performed by varying the contents of reaction mixture such as NaBH₄ (4.50 to 12.38 mM), CR (0.057 to 0.078 mM) and catalyst dose (1.2 to 2.7 mg/mL). Various other toxic dyes like MB, MG, RhB and 4-NP were also reduced successfully in the presence of biogenic CAg-nPs catalysts and NaBH₄ reductants.

3. Results and Discussion

3.1. Analysis of Biosynthesized CAg-nPs

FTIR analysis of plant extract and CAg-nPs particles was done to show the interaction between different constituents of plant extract and silver nanoparticles as shown in Figure 2. Peaks of different functional groups appeared at almost the same position in the case of both plant extract and CAg-nPs particles. Peak appeared in the range of 2900 to 3400 cm⁻¹ was due to stretching vibrations of O-H and NH₂ groups present in plant extracts in the form of alcohols, amides, amines, esters, ethers and

carboxylic acids [25]. Broadened peaks that appeared in the case of CAg-nPs particles as compared to plant extracts, relevant to stretching vibrations of these groups, are an indication of the involvement of these groups in the stabilization of fabricated silver nPs. A slight change in the peak positions of these groups in the case of CAg-nPs particles also illustrates their function as ligation agents. Bands appearing at 694.23 cm^{-1} in both plant extracts and CAg-nPs particles are an indication of the presence of aromatic hydrocarbons [39]. A peak seen at 1517.71 cm^{-1} is a characteristic signal of aromatic C=C bonds [25]. Peaks appearing at 1199.27 cm^{-1} are an indication of C–O stretching vibrations [17,40]. A peak appearing at 1638.85 cm^{-1} unveiled the vibrations of carbonyl group (C=O). Kasthuri et al. prepared biosynthesized gold and silver nanoparticle by using phyllanthin extract at room temperature and concluded that there is a formation of some sort of interaction between moieties of plant extract and metal nanoparticles by FTIR analysis [22].

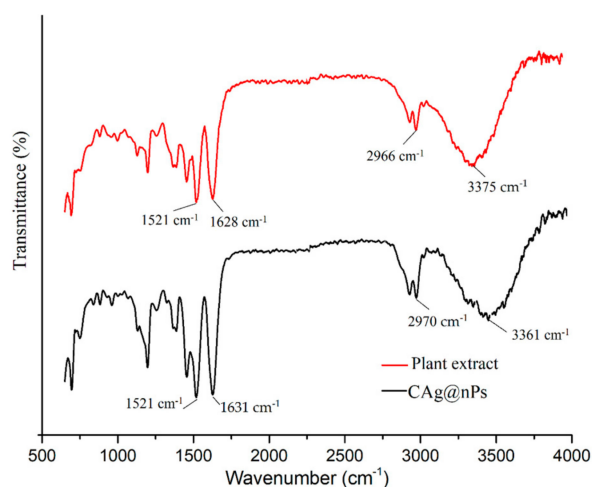


Figure 2. FTIR spectra of plant extract and biosynthesized CAg-nPs.

UV-Vis spectra of CAg-nPs particles were also obtained at different time intervals during their preparation as shown in Figure 3. At the beginning, a mixture of plant extract and silver salt showed no peak. However, a small peak with low absorbance intensity appeared 16 min after the start of reaction. This peak became sharp, distinct and less broad with progress of reaction. An absorbance intensity of the peak also increased along with its shifting toward a high wavelength (red shifting). Actually, an increase in reaction time induces nucleation of metal nanoparticles to a large amount. Free electrons present on large sized Ag-nPs oscillate with electromagnetic radiations of low energy or high wavelength. As a result, the SPR band was red shifted. The change of appearance of suspension from light yellow to light brown also illustrates the successful fabrication of CAg-nPs particles.

UV-Vis spectra of plant extracts, aqueous AgNO_3 salt and CAg-nPs particles were also recorded for comparison purposes as shown in Figure 4. No peak was seen in the case of plant extracts of aqueous solution of AgNO_3 . This shows the transparent nature of moieties of plant extract and silver nitrate salt to UV-Vis radiations. However, a sharp peak appeared at 405 nm in the case of CAg-nPs particles, which illustrates their successful fabrication. A single, sharp and prominent peak unveils the spherical shaped and narrow size distributed nPs [39]. This peak appears in the visible region due to the surface plasmon resonance (SPR) phenomenon of Ag-nPs. Actually, electrons present on the surface of nanoparticles exhibit oscillation. Oscillating electrons resonate with electromagnetic radiations of specific frequency and result in the appearance of SPR band in the visible region [41].

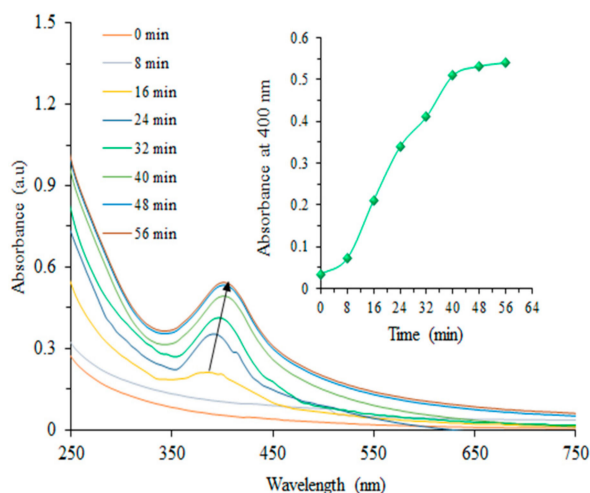


Figure 3. Time based UV-Vis spectra during preparation of biogenic CAg-nPs.

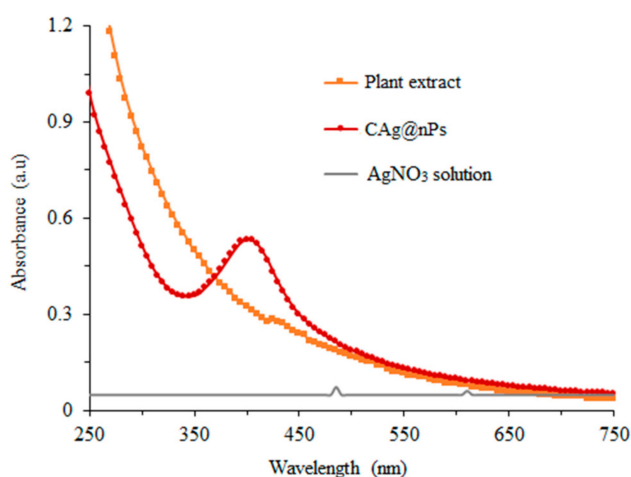


Figure 4. UV-Vis spectra of plant extract, AgNO₃ solution and CAg-nPs at room temperature.

Time based stability of biogenic CAg-nPs particles was also checked. For this purpose, spectra of freshly prepared and 15-day-old CAg-nPs particles were obtained (Figure 5a). The SPR band appeared at the same position (405 nm) with a slight decrease in the absorbance value in both cases. These results show the stability of biosynthesized CAg-nPs particles. Actually, biomolecules present in plant extracts play a role as capping/stabilizing agents and enhance the life span of silver nanoparticles [1]. Particle size distribution of CAg-nPs was evaluated by DLS analysis and spectra are shown in Figure 5b.

The average diameter of CAg-nPs particles was found as 28 nm. TGA analysis of plant extract and biosynthesized CAg-nPs was done by changing temperature from 0 to 480 °C as shown in Figure 6. TGA curves for CAg-nPs and plant extract can be divided into three stages. The first stage in TGA curve of plant extract illustrates the weight loss with temperature increase up to 100 °C because of evaporation of water contents present in plant extracts [42]. In the second stage, due to an increase of temperature up to 250 °C, there was almost no change in weight loss. During this stage, most of the heat is absorbed by the biomacromolecules to decrease the strength of intermolecular forces. In the third stage, there was a sharp decrease in weight loss due to the decomposition of plant extract contents. However, in the case of biogenic CAg-nPs catalyst, there was a steady and sharp weight loss as temperature was increased from 0 to 350 °C with respect to plant extract thermal behavior. This sharp weight loss of biogenic CAg-nPs particles may be associated with assembling Ag-nPs that promote the decomposition of plant extract contents [22]. However, weight loss was not approached to zero due to the presence of silver nanoparticles in CAg-nPs particles. Thus, less weight loss was seen in the case

of CAg-nPs particles as compared to pure plant extract at high temperature. Percentage content of Ag-nPs was also calculated by TGA analysis. It was seen that 15% silver nanoparticles were present in biosynthesized CAg-nPs as calculated from the difference of weight loss curves of CAg-nPs and of plant extract at 450 °C. Mata et al. also performed TGA analysis to study the thermal behavior of *Plumeria alba* extract treated gold nanoparticles and observed the same temperature induced weight loss trend [42]. Ayinde and coworkers investigated the size of *Citrus paradisi* peel extract induced Ag-nPs by SEM analysis [25]. The size of spherical shaped and bio-synthesized Ag-nPs was found as 14.84 nm. Kalia et al. also illuminated the shape of peel extract induced prepared Ag-nPs vis SEM analysis and observed the rod shape metal nanoparticles [43].

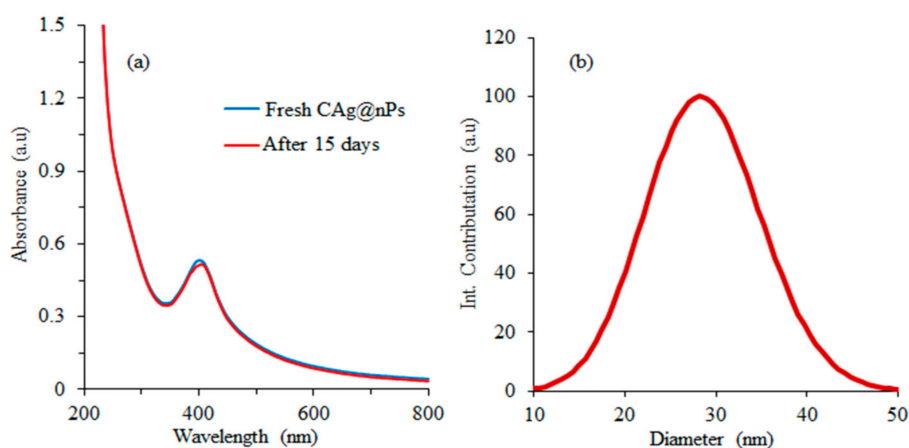


Figure 5. (a) Time dependent stability of biosynthesized CAg-nPs and (b) particle size distribution of biosynthesized CAg-nPs particles.

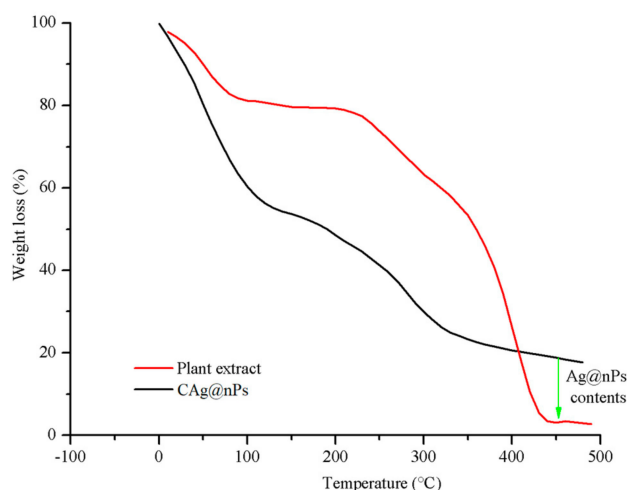


Figure 6. TGA analysis of plant extract and CAg-nPs nanoparticles.

3.2. Catalytic Reduction of Toxic Dyes

Various toxic dyes are released into water sources due to massive industrialization [44]. These dyes are stable and highly dangerous for the environment. About 10–20% of dyes are lost in wastewater streams and make their removal a major concern [45]. The best way to reduce toxic effects of these dyes is to convert them into less toxic products by using NaBH_4 as reductant. Thus, these products are alternatively reduced to further non-toxic products [46]. However, the reduction of dyes by BH_4^- ions is a thermodynamically favorable process. However, the conversion of dyes by BH_4^- ions in the absence of catalyst is kinetically unfavorable and such reactions proceed at a slow speed. This may be

due to the energy barrier present between BH_4^- ions and substrate dyes [42]. Thus, non-catalytic reduction of dyes requires more time. However, the presence of metal nanoparticles (mNPs) in reaction mixture speed up the rate of reduction of dyes which result in increased reaction efficiency. mNPs exhibit a large surface area for reactant adsorption and result in high catalytic activity for dye reduction. Actually, mNPs provide a new path for the reactants with a low level energy barrier and convert them into products easily. Thus, mNPs catalysts act as conveyor belts for electron transfer from reductant to substrate and facilitate the reduction of toxic dyes.

CR is azo dye with carcinogenic and mutagenic nature [1]. It is red in color and shows maximum absorbance at 495 nm in UV-Vis spectra. In addition, 0.060 mM CR and 7.88 mM NaBH_4 were added in quartz cells along with 1.8 mg/mL CAg-nPs catalyst and spectra were recorded (380 to 680 nm) with a time interval of one min at room temperature (Figure 7). The addition of CAg-nPs in mixture of CR and NaBH_4 leads to a decrease in absorbance intensity of the peak. Thus, the decrease in absorption intensity shows the decrease in CR concentration with the passage of time according to Beer-Lambert law [45]. Actually, the catalyst acts as a carrier to transfer hydride and electrons from borohydride to dye.

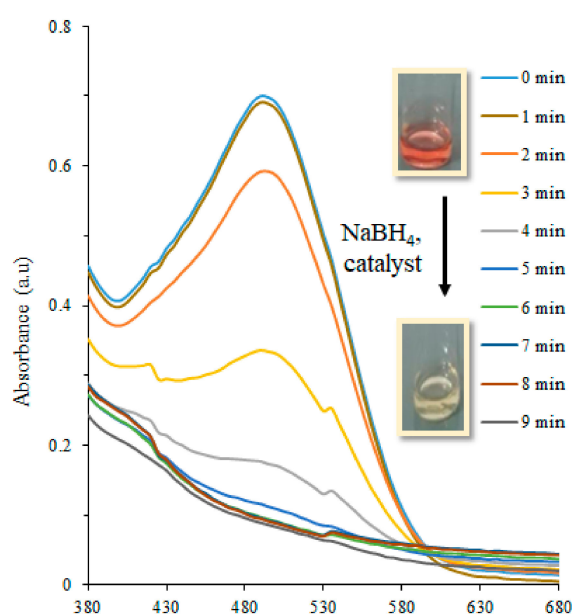


Figure 7. CR reduction in the presence of biosynthesized CAg-nPs catalyst ($[\text{CR}] = 0.060 \text{ mM}$, $[\text{NaBH}_4] = 7.88 \text{ mM}$, catalyst = 1.8 mg/mL) at ambient temperature.

The catalytic bleaching of red color of CR to white color was obtained in 9 min. The presence of CAg-nPs particles did not interfere in the monitoring of CR reduction by the spectrophotometer because the surface plasmon resonance (SPR) band of CAg-nPs particles appeared at 405 nm (Figure 4). The same reaction was also carried out as control reaction with NaBH_4 (absence of catalyst) (Figure 8a), with plant extract (in the absence of NaBH_4) (Figure 8b) and with catalyst (absence of NaBH_4) (Figure 8) to confirm whether the fading of the red color of CR was due to its degradation induced by biosynthesized CAg-nPs catalyst or adsorption by plant extract or catalyst.

Absorbance intensity of peak was slightly decreased in the presence of NaBH_4 and absence of CAg-nPs catalyst (Figure 8a). It explains the thermodynamic feasibility of reaction but the presence of large kinetic barrier between the reactants. No change in absorbance intensity of reaction mixture was observed in the presence of plant extract or Ag-nPs. These results explain that a decrease in absorbance intensity of CR or fading of its color was due to inclusion of a biogenic CAg-nPs catalyst in a reaction mixture that speeds up the rate of CR reduction in the presence of NaBH_4 . Results also explain that CR was reduced sharply in less time in the presence of catalyst rather than being adsorbed by the plant extract or Ag-nPs. Actually, reduction of CR was completed in a short time rather than being adsorbed

by the surface. Thus, this result illustrates that the decrease in absorbance intensity of dye was due to catalytic reduction rather than adsorption phenomenon.

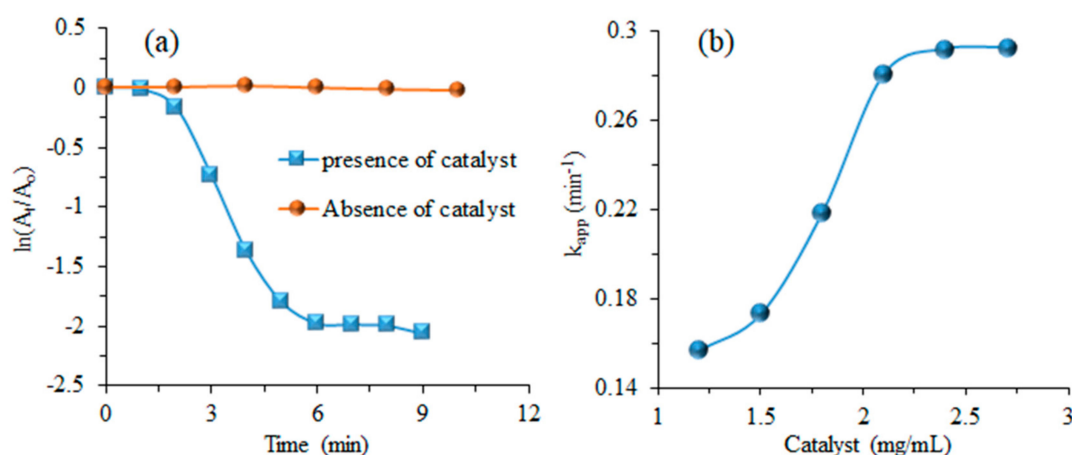


Figure 8. (a) Plot of $\ln(A_t/A_0)$ vs. time and (b) plot of catalyst dose vs. k_{app} for reduction of CR [conditions: CR = 0.045 mM, NaBH_4 = 7.88 mM] at room temperature.

3.3. Kinetic Study

Monitoring of reaction was continued until the change in absorbance of reaction mixture became constant. Due to excessive use of NaBH_4 as compared to CR ($\text{NaBH}_4/\text{CR} \geq 100$), the kinetic aspect of reduction reactions was explained by pseudo first order [$\ln(A_t/A_0)$ against time] [46]. CR was not reduced immediately after the addition of catalyst in the reaction mixture in the presence of NaBH_4 reductant. This delay in reduction of CR was due to the presence of oxygen in reaction mixtures that prevents the immediate reduction of CR. Time between adding of catalyst in reaction mixture and start of reaction is called delay time. After delay time, CR was rapidly reduced to the product in the presence of CAg-nPs catalyst and reducing agent. As the Beer–Lambert law states, the A_t (absorbance at any time) and A_0 (absorbance at zero time) are directly proportional to C_t (concentration at any time) and C_0 (concentration at zero time), respectively. Thus, the change in absorbance at λ_{max} of CR actually explains its concentration at that specific time. Pseudo first order plots for CR degradation with and without CAg-nPs biogenic catalyst are shown in Figure 8a. Values of apparent rate constant (k_{app}) for CR reduction were calculated from linear regions of plots shown in Figure 8a. k_{app} for CR degradation was found as 0.468 and 0.003 min^{-1} with and without biogenic catalyst, respectively.

Percentage conversion of CR in product was also calculated for catalytic and un-catalyzed reaction [44]. Value of percentage conversion of CR with and without CAg-nPs biogenic catalyst was found to be 87.28% and 2.62%, respectively.

Varadayenkatesan et al. prepared Ag-nPs by using the flower extract of *Thunbergia grandiflora* and employ these particles as a catalyst for reduction of CR [34]. The value of apparent rate constant (k_{app}) for reduction of CR was found as 0.0999 min^{-1} . Indana and co-workers utilized gum tragacanth fabricated Ag-nPs as a catalyst for reduction of CR using NaBH_4 as reductant [33]. The value of k_{app} was found as 0.148 min^{-1} and reaction was completed in 15 min. Thus, results showed that our reported biogenic Ag-nPs catalyst showed high activity with less reaction time and high value of k_{app} as compared to previously reported work.

3.4. Effect of Reaction Conditions

Reduction of CR was also performed by changing the concentrations of CR (0.057 to 0.078 mM) while keeping NaBH_4 and catalyst as 7.88 mM and 2.1 mg/mL , respectively. Values k_{app} , half life and reaction completion time for reduction of CR under its different concentrations are given in Table 2. It can be seen from Table 2 that the value of k_{app} was initially increased, attained the maxima and

then was decreased as CR concentration was increased. At low contents of CR, both CR molecules and BH_4^{-1} ions were adsorbed on the surface of catalyst simultaneously and results in a high value of k_{app} . However, at high concentrations of CR, most of the active sites of the catalyst are occupied by CR molecules as compared to BH_4^{-1} ions. Due to insufficient adsorbed BH_4^{-1} ions compared to CR molecules, the rate of catalytic reduction of CR was decreased. This leads to a low value of k_{app} . The plot of k_{app} vs. CR concentration for its reduction in the presence of reducing agent is shown in Figure 9a. The curve obtained for CR dependent k_{app} value shows that CR reduction followed the LH mechanism. According to this mechanism, reacting species like CR and BH_4^{-1} ions were first adsorbed on a fixed number of active sites of biogenic CAg-nPs catalyst. Then, adsorbed CR molecules and BH_4^{-1} ions reacted with each other on the surface of the catalyst, and CR was converted into environmental benign products. In the next step, adsorbed product was desorbed and diffused to bulk, making the availability of active sites for adsorption of more reacting species. Actually, biogenic CAg-nPs catalyst acts as a conveyor belt for speedy electrons transfer from BH_4^{-1} ions to CR molecules due to the large surface area of nanoparticles. Thus, a high activity of CAg-nPs catalyst lies in their efficiency during electrons transfer process [42].

Table 2. Effect of CR, NaBH_4 and catalyst contents for reduction of CR using biogenic CAg-nPs catalyst at ambient temperature.

Contents	CR (mM)	NaBH_4 (mM)	Catalyst (mg/mL)	k_{app} (min^{-1})	Half Life (min)	R^2	Induction Time (min)	Reaction Completion Time (min)
CR	0.057	7.88	2.1	0.229	3.026	0.988	2	13
	0.060	7.88	2.1	0.294	2.357	0.992	1	9
	0.063	7.88	2.1	0.544	1.274	0.951	0	4
	0.066	7.88	2.1	0.591	1.173	0.963	0	5
	0.069	7.88	2.1	0.469	1.478	0.982	1	7
	0.072	7.88	2.1	0.432	1.604	0.967	2	8
	0.075	7.88	2.1	0.404	1.715	0.995	2	9
	0.078	7.88	2.1	0.321	2.159	0.935	2	9
NaBH_4	0.072	4.50	2.1	0.156	4.442	0.972	3	27
	0.072	5.63	2.1	0.204	3.397	0.955	3	21
	0.072	6.75	2.1	0.255	2.718	0.933	1	12
	0.072	7.88	2.1	0.448	1.547	0.945	1	09
	0.072	8.33	2.1	0.390	1.777	0.9664	0	09
	0.072	9.00	2.1	0.281	2.466	0.9655	2	14
	0.072	10.13	2.1	0.249	2.783	0.9372	2	16
	0.072	11.25	2.1	0.194	3.572	0.978	2	20
Catalyst	0.072	7.88	1.2	0.157	4.414	0.997	3	26
	0.072	7.88	1.5	0.173	4.006	0.994	2	23
	0.072	7.88	1.8	0.218	3.179	0.982	1	19
	0.072	7.88	2.1	0.281	2.466	0.978	1	15
	0.072	7.88	2.4	0.292	2.373	0.995	0	14
	0.072	7.88	2.7	0.293	2.365	0.999	0	12

CR reduction was also done by varying the concentration of NaBH_4 (4.50 to 12.38 mM) while CR and catalysts were taken as 0.072 mM and 2.1 mg/mL, respectively. Values of k_{app} , reaction completion time and half life for CR reduction by using different concentrations of CR are given in Table 2. Reaction completion time for CR reduction was first decreased and then was increased as the contents of NaBH_4 in reaction mixture were increased. A trend observed for NaBH_4 dependent values of k_{app} for CR reduction was similar to that of CR concentration depending on k_{app} value. A plot of k_{app} against the concentration of NaBH_4 for CR reduction is shown in Figure 9b. k_{app} was first increased, approaching the highest values and then was increased as NaBH_4 content in reaction mixture was increased.

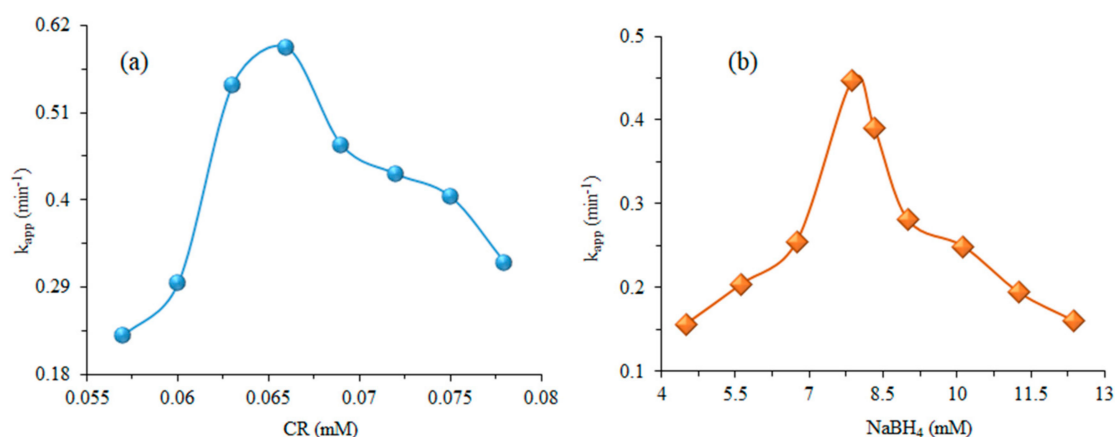


Figure 9. (a) CR concentration, (b) Sodium borohydride concentration dependent k_{app} relation for degradation of CR at ambient temperature (Reaction conditions: $[\text{NaBH}_4] = 7.88 \text{ mM}$, $[\text{CR}] = 0.072 \text{ mM}$ and catalyst = 2.1 mg/mL).

The amount of catalyst was changed from 1.2 to 2.7 mg/mL in reaction mixture while the amount of NaBH₄ and CR was kept as 7.88 and 0.072 mM, respectively, for reduction of CR. Values of k_{app} , induction time, reaction completion time and half life for CR degradation at different amounts of catalyst are given in Table 2. The value of k_{app} was increased with the increase of catalyst amount up to a limit, and then it became constant. Actually, a high catalyst dose offers a large number of active sites for the adsorption of reacting species. A high catalyst dose induced a high k_{app} value for CR reduction. At a very large amount of catalyst, all reacting species are adsorbed on the surface of the catalyst and lead to the saturation of catalyst surface. Thus, a further increase of the catalyst amount has no effect on the rate of reaction or on the value of k_{app} . As a result, the catalyst dependent value of k_{app} becomes constant at a high amount of catalyst as shown in Figure 8b. Previous studies show that catalytic reduction of dyes depends on the available active site on the surface of catalyst for adsorption of reactants as well as the number of nPs per volume. Thus, our results were found to be in agreement with the previous literature.

3.5. Reduction of Other Dyes and Nitroarenes

Various other toxic organic compounds like MG, MB, RhB and 4-NP having concentrations of 0.072 mM were also reduced individually in the presence of NaBH₄ reducing agent and CAg-nPs catalyst as shown in Figure 10. Reactions were completed in feasible time intervals and monitoring of reaction was easy while using 0.072 mM solution of all dyes individually.

Various parameters for catalytic reduction of MG, MB, RhB and p-NP are given in Table 3. It was concluded that RhB was not reduced completely in the presence of catalyst as compared to MB and RhB. The decreasing order of reduction of dyes in terms of k_{app} was MB > MG > 4-NP > RhB. A high reduction efficiency of biocatalysts for MB was due to its nature. Mb was degraded easily while the lowest reduction efficiency for RhB was due to its complex structure.

Table 3. Reduction of various dyes in the presence of CAg-nPs using NaBH₄ as reducing agent.

Dyes	k_{app} (min ⁻¹)	Intrinsic Rate Constant (mL·mg ⁻¹ ·min ⁻¹)	Reaction Completion Time (min)	Reduction Efficiency (%)
MB	0.613	0.292	4	93.29
MG	0.451	0.215	7	83.73
4-NP	0.247	0.118	9	88.90
RhB	0.085	0.041	18	60.53

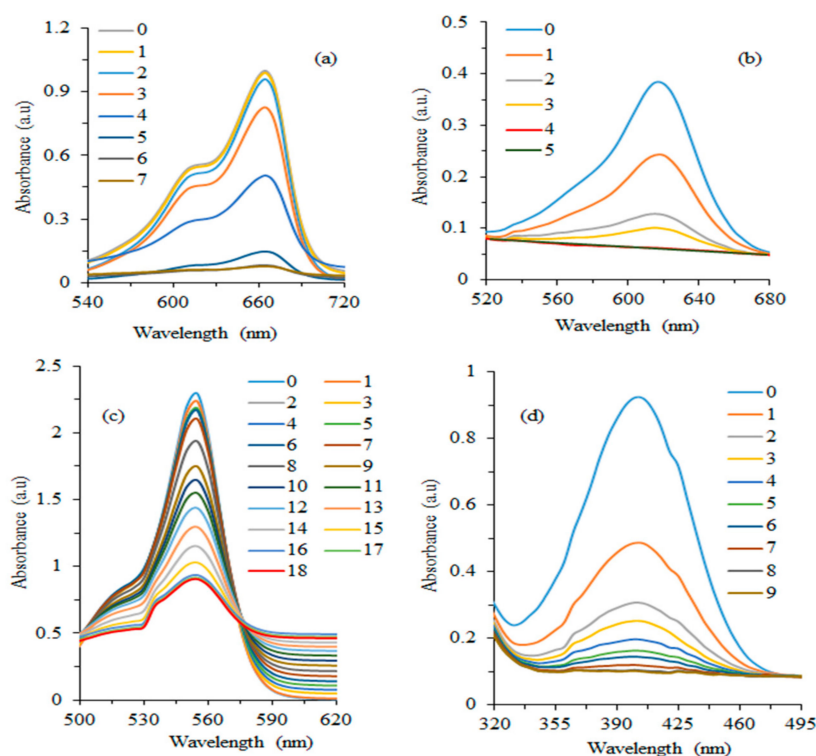


Figure 10. Catalytic reduction of various dyes (0.072 mM) such as (a) Mb, (b) MG, (c) RhB and (d) 4-Np in the presence of biogenic CAg-nPs catalyst (2.1 mg/mL) and NaBH_4 (7.88 mM) at an ambient temperature.

Catalyst was recycled from the reaction mixture by performing centrifugation at a high speed and reused for CR reduction. There was not a remarkable decrease in the reduction efficiency of the catalyst for up to three consecutive cycles (reduction efficiency $\approx 87\%$ to 82% from the 1st to 3rd cycle). Recoverability and reusability of catalyst were also investigated after three cycles. A sharp reduction in the value of percentage removal was observed. This may be due to coagulation of Ag-nPs due to repeated usage. Reduction efficiency of the biogenic CAg-nPs catalyst for different reusability cycles for CR reduction is shown in Figure 11.

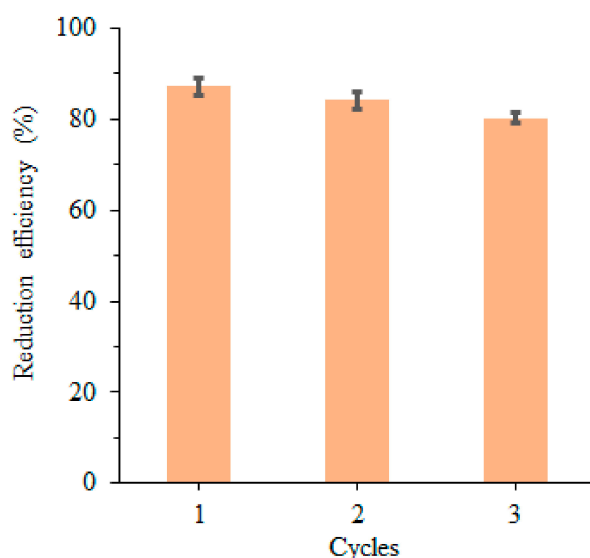


Figure 11. Recyclability of biogenic CAg-nPs catalyst for reduction of CR (0.216 mM) in the presence of NaBH_4 (24.03 mM) and catalyst (8.42 mg/mL) at an ambient temperature.

4. Conclusions

This study presents the ecofriendly biogenic synthesis of CAg-nPs by an aqueous peel extract of *Citrus paradise*. FTIR and UV-Vis analysis demonstrates the involvement of different metabolites of plant extract in the bio-reduction process and stabilization of silver nPs. UV-Vis analysis also confirms the successful fabrication of silver nanoparticles along with their spherical shape and narrow size distribution. TGA analysis shows that the prepared biogenic CAg-nPs catalyst is incorporated with 15% silver nanoparticle contents. Catalytic activity of biogenic CAg-nPs was explored against the reduction of various toxic dyes such as CR, MB, MG, RhB and 4-NP using BH_4^{-1} ions as hydrogen/electrons source. Results prove the remarkable catalytic efficiency of biogenic CAg-nPs nano-catalysts for reduction of reported dyes. The CAg-nPs catalyst was conveniently recovered from a reaction mixture by high speed centrifugation and applied for subsequent reaction without a remarkable decrease in its activity.

The CAg-nPs catalyst was applied to speed up the rate of reduction of selective dyes. However, textile industry wastewater contains a lot of other toxic chemicals. The effect of those chemicals on the activity of catalysts can also be addressed to make it effective for treatment of industrial wastewater.

Author Contributions: Conceptualization, K.N. and A.A.; Methodology, A.A.; Software, M.Z.U.R.; Validation, K.N. and D.D.; Formal Analysis, T.S.A.; Investigation, A.A.; Resources, T.S.A.; Data Curation, K.N.; Writing—Original Draft Preparation, K.N.; Writing—Review & Editing, A.A.; Visualization, D.D.; Supervision, D.D.; Project Administration, M.Z.U.R.; Funding Acquisition, T.S.A. All authors have read and agreed to the published version of the manuscript.

Funding: This work was funded by the Researchers Supporting Project Number (RSP-2020/254) King Saud University, Riyadh, Saudi Arabia.

Conflicts of Interest: The authors declare no conflict of interest.

References

1. Naseem, K.; Farooqi, Z.H.; Begum, R.; Irfan, A. Removal of Congo red dye from aqueous medium by its catalytic reduction using sodium borohydride in the presence of various inorganic nano-catalysts: A review. *J. Clean. Prod.* **2018**, *187*, 296–307. [[CrossRef](#)]
2. Zhang, X.; Xu, P.; Liu, G.; Ahmad, A.; Chen, X.; Zhu, Y.; Alothman, A.; Hussain, S.; Qiao, G. Synthesis, characterization and wettability of Cu–Sn alloy on the Si-implanted 6H–SiC. *Coatings* **2020**, *9*, 906. [[CrossRef](#)]
3. Albukhari, S.M.; Ismail, M.; Akhtar, K.; Danish, E.Y. Catalytic reduction of nitrophenols and dyes using silver nanoparticles@ cellulose polymer paper for the resolution of waste water treatment challenges. *Colloids Surf. Physicochem. Eng. Asp.* **2019**, *577*, 548–561. [[CrossRef](#)]
4. Aravind, M.; Ahmad, A.; Ahmad, I.; Amalanathan, M.; Naseem, K.; Mary, S.M.M.; Parvathiraja, C.; Hussain, S.; Algarni, T.S.; Pervaiz, M.; et al. Critical green routing synthesis of silver NPs using jasmine flower extract for biological activities and photocatalytic degradation of methylene blue. *J. Environ. Chem. Eng.* **2020**, 104877. [[CrossRef](#)]
5. Hussain, S.; Khan, A.J.; Arshad, M.; Javed, M.S.; Ahmad, A.; Shah, S.S.A.; Khan, M.R.; Akram, S.; Zulfiqar, Ali, S.; et al. Charge storage in binder-free 2D-hexagonal CoMoO_4 nanosheets as a redox active material for pseudocapacitors. *Ceram. Int.* **2020**. [[CrossRef](#)]
6. Naseem, K.; Farooqi, Z.H.; Begum, R.; Ghufuran, M.; Rehman, M.Z.U.; Najeeb, J.; Irfan, A.; Al-Sehemi, A.G. Poly (N-isopropylmethacrylamide-acrylic acid) microgels as adsorbent for removal of toxic dyes from aqueous medium. *J. Mol. Liq.* **2018**, *268*, 229–238. [[CrossRef](#)]
7. Ahmad, A.; Jini, D.; Aravind, M.; Parvathiraja, C.; Ali, R.; Kiyani, M.Z.; Alothman, A. A novel study on synthesis of egg shell based activated carbon for degradation of methylene blue via photocatalysis. *Arab. J. Chem.* **2020**. [[CrossRef](#)]
8. Ahmad, A.; Mubharak, N.M.; Naseem, K.; Tabassum, H.; Rizwan, M.; Najda, A.; Kashif, M.; Bin-Jumah, M.; Hussain, A.; Shaheen, A.; et al. Recent advancement and development of chitin and chitosan-based nanocomposite for drug delivery: Critical approach to clinical research. *Arab. J. Chem.* **2020**, *13*, 8935–8964. [[CrossRef](#)]

9. Suresh, M.; Sivasamy, A. Fabrication of graphene nanosheets decorated by nitrogen-doped ZnO nanoparticles with enhanced visible photocatalytic activity for the degradation of Methylene Blue dye. *J. Mol. Liq.* **2020**, *317*, 114112. [[CrossRef](#)]
10. Ganapuram, B.R.; Alle, M.; Dadigala, R.; Dasari, A.; Maragoni, V.; Guttena, V. Catalytic reduction of methylene blue and Congo red dyes using green synthesized gold nanoparticles capped by salmalia malabarica gum. *Int. Nano Lett.* **2015**, *5*, 215–222. [[CrossRef](#)]
11. Naseem, K.; Begum, R.; Wu, W.; Irfan, A.; Al-Sehemi, A.G.; Farooqi, Z.H. Catalytic reduction of toxic dyes in the presence of silver nanoparticles impregnated core-shell composite microgels. *J. Clean. Prod.* **2019**, *211*, 855–864. [[CrossRef](#)]
12. Lu, Y.; Proch, S.; Schrinner, M.; Drechsler, M.; Kempe, R.; Ballauff, M. Thermosensitive core-shell microgel as a “nanoreactor” for catalytic active metal nanoparticles. *J. Mater. Chem.* **2009**, *19*, 3955–3961. [[CrossRef](#)]
13. Graça, C.A.; Mendes, M.A.; Teixeira, A.C.S.; de Velosa, A.C. Anoxic degradation of chlorpyrifos by zerovalent monometallic and bimetallic particles in solution. *Chemosphere* **2020**, *244*, 125461. [[CrossRef](#)]
14. Kashif, M.; Ngaini, Z.; Harry, A.V.; Vekariya, R.L.; Ahmad, A.; Zuo, Z.; Sahari, S.K.; Hussain, S.; Khan, Z.A.; Alarifi, A. An experimental and DFT study on novel dyes incorporated with natural dyes on titanium dioxide (TiO₂) towards solar cell application. *Appl. Phys. A* **2020**, *126*, 1–13. [[CrossRef](#)]
15. Zhang, J.; Ma, N.; Tang, F.; Cui, Q.; He, F.; Li, L. pH-and glucose-responsive core-shell hybrid nanoparticles with controllable metal-enhanced fluorescence effects. *ACS Appl. Mater. Interfaces* **2012**, *4*, 1747–1751. [[CrossRef](#)]
16. Shameli, K.; Ahmad, M.B.; Zamanian, A.; Sangpour, P.; Shabanzadeh, P.; Abdollahi, Y.; Zargar, M. Green biosynthesis of silver nanoparticles using Curcuma longa tuber powder. *Int. J. Nanomed.* **2012**, *7*, 5603. [[CrossRef](#)]
17. Rostami-Vartooni, A.; Nasrollahzadeh, M.; Alizadeh, M. Green synthesis of seashell supported silver nanoparticles using Bunium persicum seeds extract: Application of the particles for catalytic reduction of organic dyes. *J. Colloid Interface Sci.* **2016**, *470*, 268–275. [[CrossRef](#)]
18. Naseem, K.; Farooqi, Z.H.; Begum, R.; Wu, W.; Irfan, A.; Ajmal, M. Systematic study for catalytic degradation of nitrobenzene derivatives using core@ shell composite micro particles as catalyst. *Colloids Surf. Physicochem. Eng. Asp.* **2020**, *594*, 124646. [[CrossRef](#)]
19. Tang, F.; Ma, N.; Tong, L.; He, F.; Li, L. Control of metal-enhanced fluorescence with pH-and thermoresponsive hybrid microgels. *Langmuir* **2012**, *28*, 883–888. [[CrossRef](#)]
20. Abbasi, E.; Milani, M.; Fekri Aval, S.; Kouhi, M.; Akbarzadeh, A.; Tayefi Nasrabadi, H.; Nikasa, P.; Joo, S.W.; Hanifehpour, Y.; Nejati-Koshki, K. Silver nanoparticles: Synthesis methods, bio-applications and properties. *Crit. Rev. Microbiol.* **2016**, *42*, 173–180. [[CrossRef](#)]
21. Nava, O.; Soto-Robles, C.; Gómez-Gutiérrez, C.; Vilchis-Nestor, A.; Castro-Beltrán, A.; Olivas, A.; Luque, P. Fruit peel extract mediated green synthesis of zinc oxide nanoparticles. *J. Mol. Struct.* **2017**, *1147*, 1–6. [[CrossRef](#)]
22. Kasthuri, J.; Kathiravan, K.; Rajendiran, N. Phyllanthin-assisted biosynthesis of silver and gold nanoparticles: A novel biological approach. *J. Nanopart. Res.* **2009**, *11*, 1075–1085. [[CrossRef](#)]
23. Shankar, S.S.; Rai, A.; Ahmad, A.; Sastry, M. Rapid synthesis of Au, Ag, and bimetallic Au core-Ag shell nanoparticles using Neem (Azadirachta indica) leaf broth. *J. Colloid Interface Sci.* **2004**, *275*, 496–502. [[CrossRef](#)]
24. Gardea-Torresdey, J.; Parsons, J.; Gomez, E.; Peralta-Videa, J.; Troiani, H.; Santiago, P.; Yacaman, M.J. Formation and growth of Au nanoparticles inside live alfalfa plants. *Nano Lett.* **2002**, *2*, 397–401. [[CrossRef](#)]
25. Ayinde, W.; Gitari, W.; Samie, A. Optimization of microwave-assisted synthesis of silver nanoparticle by Citrus paradisi peel and its application against pathogenic water strain. *Green Chem. Lett. Rev.* **2019**, *12*, 225–234. [[CrossRef](#)]
26. Najafinejad, M.S.; Mohammadi, P.; Afsahi, M.M.; Sheibani, H. Green synthesis of the Fe₃O₄@polythiophen-Ag magnetic nanocatalyst using grapefruit peel extract: Application of the catalyst for reduction of organic dyes in water. *J. Mol. Liq.* **2018**, *262*, 248–254. [[CrossRef](#)]
27. Kumar, B.; Smita, K.; Galeas, S.; Sharma, V.; Guerrero, V.H.; Debut, A.; Cumbal, L. Characterization and application of biosynthesized iron oxide nanoparticles using Citrus paradisi peel: A sustainable approach. *Inorg. Chem. Commun.* **2020**, *119*, 108116. [[CrossRef](#)]
28. Kumar, B.; Smita, K.; Cumbal, L.; Debut, A. Green approach for fabrication and applications of zinc oxide nanoparticles. *Bioinorg. Chem. Appl.* **2014**, *2014*, 523869. [[CrossRef](#)]
29. Soto, K.M.; Quezada-Cervantes, C.T.; Hernández-Iturriaga, M.; Luna-Bárcenas, G.; Vazquez-Duhalt, R.; Mendoza, S. Fruit peels waste for the green synthesis of silver nanoparticles with antimicrobial activity against foodborne pathogens. *LWT* **2019**, *103*, 293–300. [[CrossRef](#)]

30. Jackson, T.C.; Uwah, T.O.; Ifekpolugo, N.L.; Emmanuel, N.A. Comparison of antimicrobial activities of silver nanoparticles biosynthesized from some Citrus species. *Am. J. Nano Res. Appl.* **2018**, *6*, 54–59.
31. Vankar, P.S.; Shukla, D. Biosynthesis of silver nanoparticles using lemon leaves extract and its application for antimicrobial finish on fabric. *Appl. Nanosci.* **2012**, *2*, 163–168. [[CrossRef](#)]
32. Barbinta-Patrascu, M.E.; Badea, N.; Ungureanu, C.; Iordache, S.M.; Constantin, M.; Purcar, V.; Rau, I.; Pirvu, C. Ecobiophysical aspects on nanosilver biogenerated from citrus reticulata peels, as potential biopesticide for controlling pathogens and wetland plants in aquatic media. *J. Nanomater.* **2017**, *2017*, 4214017. [[CrossRef](#)]
33. Indana, M.K.; Gangapuram, B.R.; Dadigala, R.; Bandi, R.; Guttena, V. A novel green synthesis and characterization of silver nanoparticles using gum tragacanth and evaluation of their potential catalytic reduction activities with methylene blue and Congo red dyes. *J. Anal. Sci. Technol.* **2016**, *7*, 19. [[CrossRef](#)]
34. Varadavenkatesan, T.; Selvaraj, R.; Vinayagam, R. Green synthesis of silver nanoparticles using Thunbergia grandiflora flower extract and its catalytic action in reduction of Congo red dye. *Mater. Today Proc.* **2020**, *23*, 39–42. [[CrossRef](#)]
35. Saha, J.; Begum, A.; Mukherjee, A.; Kumar, S. A novel green synthesis of silver nanoparticles and their catalytic action in reduction of Methylene Blue dye. *Sustain. Environ. Res.* **2017**, *27*, 245–250. [[CrossRef](#)]
36. Naraginti, S.; Sivakumar, A. Eco-friendly synthesis of silver and gold nanoparticles with enhanced bactericidal activity and study of silver catalyzed reduction of 4-nitrophenol. *Spectrochim. Acta Part A Mol. Biomol. Spectrosc.* **2014**, *128*, 357–362. [[CrossRef](#)]
37. Dauthal, P.; Mukhopadhyay, M. Prunus domestica fruit extract-mediated synthesis of gold nanoparticles and its catalytic activity for 4-nitrophenol reduction. *Ind. Eng. Chem. Res.* **2012**, *51*, 13014–13020. [[CrossRef](#)]
38. Kahsay, M.H.; RamaDevi, D.; Kumar, Y.P.; Mohan, B.S.; Tadesse, A.; Battu, G.; Basavaiah, K. Synthesis of silver nanoparticles using aqueous extract of Dolichos lablab for reduction of 4-Nitrophenol, antimicrobial and anticancer activities. *OpenNano* **2018**, *3*, 28–37. [[CrossRef](#)]
39. Kumar, P.; Govindaraju, M.; Senthamilselvi, S.; Premkumar, K. Photocatalytic degradation of methyl orange dye using silver (Ag) nanoparticles synthesized from Ulva lactuca. *Colloids Surf. B Biointerfaces* **2013**, *103*, 658–661. [[CrossRef](#)]
40. Begum, R.; Naseem, K.; Ahmed, E.; Sharif, A.; Farooqi, Z.H. Simultaneous catalytic reduction of nitroarenes using silver nanoparticles fabricated in poly (N-isopropylacrylamide-acrylic acid-acrylamide) microgels. *Colloids Surf. Physicochem. Eng. Asp.* **2016**, *511*, 17–26. [[CrossRef](#)]
41. Farooqi, Z.H.; Naseem, K.; Begum, R.; Ijaz, A. Catalytic reduction of 2-nitroaniline in aqueous medium using silver nanoparticles functionalized polymer microgels. *J. Inorg. Organomet. Polym. Mater.* **2015**, *25*, 1554–1568. [[CrossRef](#)]
42. Mata, R.; Bhaskaran, A.; Sadras, S.R. Green-synthesized gold nanoparticles from Plumeria alba flower extract to augment catalytic degradation of organic dyes and inhibit bacterial growth. *Particuology* **2016**, *24*, 78–86. [[CrossRef](#)]
43. Kalia, A.; Manchanda, P.; Bhardwaj, S.; Singh, G. Biosynthesized silver nanoparticles from aqueous extracts of sweet lime fruit and callus tissues possess variable antioxidant and antimicrobial potentials. *Inorg. Nano Met. Chem.* **2020**, *50*, 1–10. [[CrossRef](#)]
44. Naseem, K.; Farooqi, Z.H.; Begum, R.; Wu, W.; Irfan, A.; Al-Sehemi, A.G. Silver Nanoparticles Engineered Polystyrene-Poly (N-isopropylmethacrylamide-acrylic acid) Core Shell Hybrid Polymer Microgels for Catalytic Reduction of Congo Red. *Macromol. Chem. Phys.* **2018**, *219*, 1800211. [[CrossRef](#)]
45. Alzahrani, H.A.; Buckingham, M.A.; Wardley, W.P.; Tilley, R.D.; Ariotti, N.; Aldous, L. Gold nanoparticles immobilised in a superabsorbent hydrogel matrix: Facile synthesis and application for the catalytic reduction of toxic compounds. *Chem. Commun.* **2020**, *56*, 1263–1266. [[CrossRef](#)]
46. Ismail, M.; Khan, M.; Khan, M.A.; Akhtar, K.; Asiri, A.M.; Khan, S.B. Plant-supported silver nanoparticles: Efficient, economically viable and easily recoverable catalyst for the reduction of organic pollutants. *Appl. Organomet. Chem.* **2019**, *33*, e4971. [[CrossRef](#)]

Publisher's Note: MDPI stays neutral with regard to jurisdictional claims in published maps and institutional affiliations.



© 2020 by the authors. Licensee MDPI, Basel, Switzerland. This article is an open access article distributed under the terms and conditions of the Creative Commons Attribution (CC BY) license (<http://creativecommons.org/licenses/by/4.0/>).